The mass-metallicity-kinematics relation of the stellar components of EAGLE galaxies

L.J. Zenocratti[1,2], M.E. De Rossi[3,4], M.A. Lara-López[5] & T. Theuns[6]

[1] *Facultad de Ciencias Astronómicas y Geofísicas, UNLP, Argentina*
[2] *Instituto de Astrofísica de La Plata, CONICET–UNLP, Argentina*
[3] *Instituto de Astronomía y Física del Espacio, CONICET–UBA, Argentina*
[4] *Facultad de Ciencias Exactas y Naturales, UBA, Argentina*
[5] *Dark Cosmology Centre, University of Copenhagen, Dinamarca*
[6] *Institute for Computational Cosmology, University of Durham, Reino Unido*

Contact / ljzenocratti@gmail.com

Resumen / En este trabajo, estudiamos la relación masa estelar – metalicidad estelar como función de la cinemática interna y de la morfología en galaxias de la simulación cosmológica EAGLE. De acuerdo a lo que encontramos, para una dada masa estelar ($M_\star$), la metalicidad estelar muestra una dependencia secundaria con la morfología y la cinemática de las galaxias, que es más evidente hacia altas masas. En el extremo de altas masas ($M_\star \gtrsim 10^{10}$ M$_\odot$), aquellos sistemas soportados por dispersión de velocidades muestran en promedio menores metalicidades. Adicionalmente, galaxias de baja masa con mayor soporte rotacional son algo más pobres en metales. Las galaxias más masivas tienden a presentar morfologías más planas, siendo los sistemas prolados menos enriquecidos en promedio. A medida que el redshift z aumenta, las anteriores dependencias de la metalicidad con la morfo-cinemática se vuelven más fuertes a altas masas. Estas tendencias son consistentes con las dependencias de la relación masa estelar – metalicidad de gas con la fracción de gas, tasa de formación estelar y edad estelar, y la relación de estas últimas cantidades con la morfocinemática de las galaxias.

Abstract / In this work, we study the stellar mass – stellar metallicity relation as a function of the morpho-kinematics of galaxies in EAGLE cosmological simulations. According to our findings, at a given stellar mass ($M_\star$), stellar metallicity shows a secondary dependence on the morpho-kinematics of galaxies, which is more evident towards high masses. At the high-mass end ($M_\star \gtrsim 10^{10}$ M$_\odot$), dispersion-supported systems show lower metallicities, on average. In addition, low-mass galaxies with higher rotational support are somewhat more metal-poor. More massive galaxies tend to exhibit flatter morphologies, being prolate systems less metal-enriched, on average. As the redshift z increases, those aforementioned dependences of metallicity on kinematics and morphology tend to become stronger at high masses. These trends are consistent with the dependences of the stellar mass – gas-phase metallicity relation on gas fraction, star formation rate and stellar age, and the relation of the latter quantities with galaxy morpho-kinematics.

Keywords / galaxies: abundances — galaxies: evolution — galaxies: high-redshift — galaxies: star formation — cosmology: theory

1. Introduction

At redshift $z = 0$, the gas-phase metallicity of galaxies (Z) tends to increase with stellar mass ($M_\star$), following roughly a power law, $Z \propto M_\star^{2/5}$, with the slope of the relation flattening towards higher masses. This mass-metallicity relation (hereafter, MZR) has been studied comprehensively in the last decades, both observationally (e.g. Tremonti et al., 2004; Lara-López et al., 2010) and theoretically (e.g. Calura et al., 2009; De Rossi et al., 2015; De Rossi et al., 2017; Sharma & Theuns, 2019). In addition, there is evidence suggesting that this power-law trend is also followed by galaxies at higher redshifts, but possibly with different slope and normalization (e.g. Troncoso et al., 2014).

It is known that the scatter along the observed MZR correlates with other properties of galaxies. Ellison et al. (2008) showed that at fixed stellar mass, observed galaxies with lower specific star formation rates ($sSFR$) or smaller half-mass radii tend to have higher oxygen abundances (O/H). Lara-López et al. (2010) and Mannucci et al. (2010) reported a 3-D relationship between $M_\star$, O/H and star formation rate (SFR), according to which systems with higher $SFRs$ tend to have lower O/H at a given $M_\star$. Moreover, the latter relation could arise from a more fundamental relation between $M_\star$, metallicity and gas fraction (f_g), given the correlation between that last quantity and SFR (e.g. Bothwell et al., 2013; Lara-López et al., 2013). Also, recent observations suggest that at fixed $M_\star$, metallicity tends to be lower in galaxies with higher concentration or higher Sérsic indexes (e.g. Wu et al., 2019), although large uncertainties remain when inferring physical relations from the data.

Zenocratti et al. (2020) studied the relation between stellar mass, *gas-phase metallicity* and internal morpho-kinematics of galaxies in the EAGLE cosmological hydrodynamical simulations (Schaye et al., 2015; Crain et al., 2015), and found trends not previously reported in the

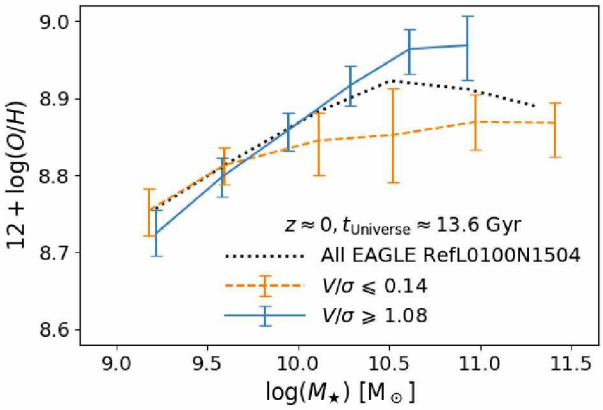

Figure 1: Stellar mass – stellar metallicity relation at redshift $z = 0$. The dotted-black lines show the median relation for our complete sample of EAGLE Ref-L0100N1504 galaxies. The coloured lines correspond to the relation binned by rotation-to-dispersion velocity ratio V/σ, for two extreme sub-samples of galaxies (dispersion-supported and rotation-supported systems, dashed-orange and solid-blue lines, respectively). Error bars encompass the $25^{\rm th}$ and $75^{\rm th}$ corresponding percentiles.

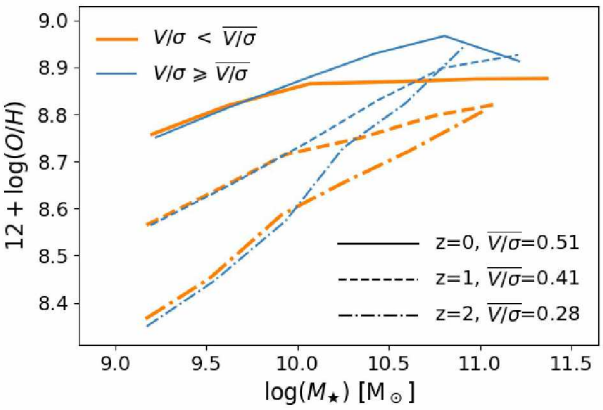

Figure 2: Stellar mass – stellar metallicity relations at different redshifts z, as indicated in the figure, for EAGLE Ref-L0100N1504 simulation galaxies. Curves representing galaxies with rotational support below the median at the given z are plotted with thick orange lines, while those with higher V/σ are plotted with thin blue lines.

literature. In this work, we extend the aforementioned analysis, studying the dependence of the stellar mass-*stellar metallicity* relation on morpho-kinematics of EAGLE galaxies. The goal of this article is to address if the scaling relation based on stellar metallicity follows the same behaviour as the one based on gas-phase metallicity. We found a resembling correlation between stellar mass and stellar metallicity, with a similar secondary dependence on morpho-kinematics, again not previously reported in mass-metallicity studies.

2. The EAGLE simulations

In this work, we use galaxies extracted from EAGLE (Evolution and Assembly of GaLaxies and their Environments) suite of cosmological hydrodynamical simulations (Schaye et al., 2015). These galaxies were generated using a modified version of the GADGET-3 code (Springel, 2005), with sub-grid physics calibrated to reproduce the $z \approx 0$ galaxy stellar mass function and the relation between galaxy mass and size, among others (Crain et al., 2015). A standard ΛCDM cosmology was adopted for EAGLE simulations, using the cosmological parameters given by the Planck Collaboration (2015): $\Omega_{\rm L} = 0.693$, $\Omega_{\rm m} = 0.307$, $\Omega_{\rm b} = 0.048$, and $h = 0.6777$. As in Zenocratti et al. (2020), we use here the reference, intermediate-resolution EAGLE simulation ("Ref-L0100N1504"), which has a co-moving extent of $L = 100$ cMpc, with an initial baryonic particle mass of 1.2×10^6 M$_\odot$ (corresponding to 1504^3 particles) and a maximum proper softening length of 0.70 pkpc. We checked that the results presented in this work are consistent with those obtained when using the recalibrated, high-resolution EAGLE "Recal-L025N0752" simulation, analysed previously by De Rossi et al. (2017).

3. Galaxy selection

Dark matter halos are identified using the FoF algorithm (Davis et al., 1985), while the SUBFIND algorithm (Springel, 2005; Dolag et al., 2009) allows to identify the sub-halos that host galaxies, which correspond to "self-bound" sub-structures of gas, stars and dark matter particles. Here we analyse properties of central galaxies (i.e. dominant galaxies of FoF halos), measuring baryonic properties within spherical apertures of 30 pkpc. We use the O/H stellar abundance to quantify stellar metallicities. In order to compare our results with Zenocratti et al. (2020), we use their galaxy selection criteria*, with our sample containing 6367 simulated galaxies. The parameters we used to characterize stellar morphology and kinematics are described in Thob et al. (2019): fraction of kinetic energy invested in ordered co-rotation ($\kappa_{\rm co}$), disc-to-total stellar mass ratio (D/T), ratio of stellar rotation to velocity dispersion (V/σ), ellipticity of the stellar body ($\epsilon_\star$), and triaxiality (T).

4. Results

Fig. 1 shows the stellar mass – stellar metallicity relation at $z = 0$, with galaxies binned by two extremes ranges of the kinematical parameter V/σ. Galaxies with stellar mass $M_\star \lesssim 10^{10}$ M$_\odot$ that are dispersion-supported (low V/σ) have on average a little higher O/H than rotationally supported systems of the same $M_\star$. O/H tends to increase with $M_\star$ in both sub-samples, but the trend is more pronounced for rotationally supported galaxies. Therefore, the trend of stellar O/H with V/σ inverts at $M_\star \gtrsim 10^{10}$ M$_\odot$, where dispersion-supported galaxies have lower metallicities than rotation-supported ones. Similar trends were found in EAGLE "Recal-L025N0752" simulation. Our results using the stellar metallicity are consistent

*We select galaxies with stellar masses $M_\star \geqslant 10^9$ M$_\odot$, and with at least 25 star-forming gas particles (gas mass of at least 5.25×10^7 M$_\odot$).

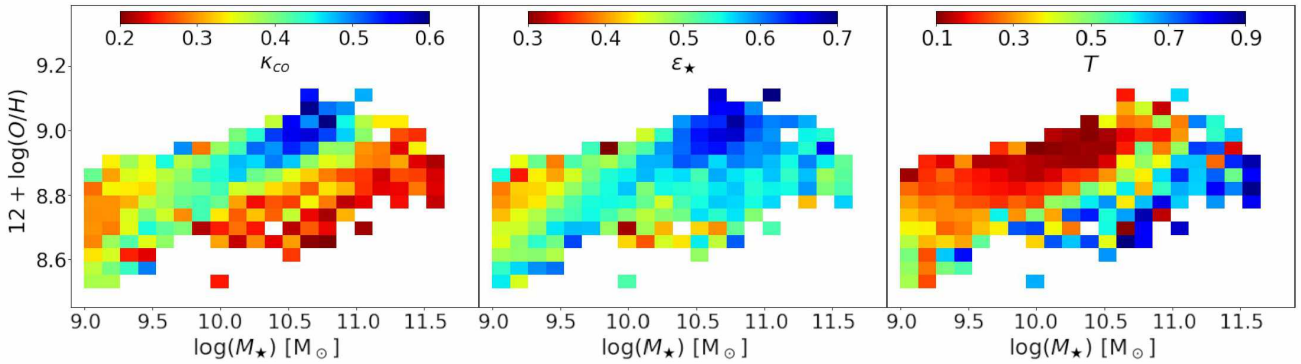

Figure 3: Stellar O/H as a function of stellar mass, for $z = 0$ EAGLE Ref-L0100N1504 simulation galaxies. Bins in O/H-$M_\star$ plane are colour-coded according to the median value of rotation-to-total energy ratio κ_{co} (*left panel*), stellar ellipticity $\epsilon_\star$ (*middle panel*) and the galaxy's triaxiality parameter T (*right panel*).

with those of Zenocratti et al. (2020) regarding the gas-phase metallicity.

In Fig. 2, the stellar mass – stellar metallicity relation at different redhifts z is shown. At a given z, the sample of simulated galaxies is separated in two subsamples according to the corresponding median value of V/σ. As expected, the normalization of the relation decreases with z, but the behaviour is quite similar: there is a clear increase of O/H with $M_\star$ for galaxies more supported by rotation, but this trend is less pronounced for galaxies with low V/σ. As z increases, the secondary dependence of O/H on kinematics tends to become stronger at $M_\star \gtrsim 10^{10}$ M$_\odot$. Similar trends with redshift are obtained when using other morpho-kinematical indicators.

Panels in Fig. 3 show the stellar O/H vs. $M_\star$ plane at $z = 0$ for our simulated sample of galaxies, colour-coding rectangular bins according to the median values of $\kappa_{\rm co}$ (left), $\epsilon_\star$ (middle), and T (right). As can be seen, at $M_\star \gtrsim 10^{10}$ M$_\odot$, more rotation-supported galaxies have higher metallicities and more flattened morphologies, showing lower triaxialities. On the other hand, at $M_\star \lesssim 10^{10}$ M$_\odot$, the trends are less evident, but galaxies with higher metallicities tend to exhibit lower values of $\kappa_{\rm co}$ and more spheroidal morphologies at a fixed $M_\star$. At intermediate masses ($M_\star \sim 10^{10}$ M$_\odot$), there is relatively little variation in $\kappa_{\rm co}$ or $\epsilon_\star$.

5. Summary and work in progress

We analysed the stellar mass – stellar metallicity relation as function of morpho-kinematical parameters in the EAGLE cosmological hydrodynamical simulations, extending the studies carried out by Zenocratti et al. (2020). At $z = 0$, we found secondary dependences of metallicity on the internal kinematics and morphology of simulated galaxies. At low masses ($M_\star \lesssim 10^{10}$ M$_\odot$), higher metallicities are found for galaxies with more spheroidal morphologies and with lower rotational support; this trend inverts at high masses ($M_\star \gtrsim 10^{10}$ M$_\odot$). At higher redshifts, the secondary O/H dependence on morpho-kinematics becomes stronger for more massive galaxies. These results and trends are consistent with secondary dependences of gas-phase O/H (at a fixed mass) on gas fraction, star formation rate and stellar age studied by De Rossi et al. (2017). A detailed analysis of the origin and evolution of the mass-metallicity – morpho-kinematics relation in EAGLE galaxies is being carried out (Zenocratti et al., in prep.), in order to better understand the set up of this correlations.

Acknowledgements: We acknowledge the Asociación Argentina de Astronomía for allowing us to communicate our results. LJZ and MEDR acknowledge support from PICT-2015-3125 of ANPCyT, PIP 112- 201501-00447 of CONICET and UNLP G151 of UNLP (Argentina). MALL is a DARK-Carlsberg Foundation Fellow (Semper Ardens project CF15-0384). We acknowledge the Virgo Consortium for making their simulation data available. The EAGLE simulations were performed using the DiRAC-2 facility at Durham, managed by the ICC, and the PRACE facility Curie based in France at TGCC, CEA, Bruyères-le-Châtel. This work used the DiRAC@Durham facility managed by the Institute for Computational Cosmology on behalf of the STFC DiRAC HPC Facility (`www.dirac.ac.uk`). The equipment was funded by BEIS capital funding via STFC capital grants ST/P002293/1, ST/R002371/1 and ST/S002502/1, Durham University and STFC operations grant ST/R000832/1. DiRAC is part of the National e-Infrastructure.

References

Bothwell M.S., et al., 2013, MNRAS, 433, 1425
Calura F., et al., 2009, A&A, 504, 373
Crain R.A., et al., 2015, MNRAS, 450, 1937
Davis M., et al., 1985, ApJ, 292, 371
De Rossi M.E., et al., 2015, MNRAS, 452, 486
De Rossi M.E., et al., 2017, MNRAS, 472, 3354
Dolag K., et al., 2009, MNRAS, 399, 497
Ellison S.L., et al., 2008, ApJL, 672, L107
Lara-López M.A., López-Sánchez Á.R., Hopkins A.M., 2013, ApJ, 764, 178
Lara-López M.A., et al., 2010, A&A, 521, L53
Mannucci F., et al., 2010, MNRAS, 408, 2115
Planck Collaboration, 2015, A&A, 594, A13
Schaye J., et al., 2015, MNRAS, 446, 521
Sharma M., Theuns T., 2019, MNRAS, 492, 2418
Springel V., 2005, MNRAS, 364, 1105
Thob A.C.R., et al., 2019, MNRAS, 485, 972
Tremonti C.A., et al., 2004, ApJ, 613, 898
Troncoso P., et al., 2014, A&A, 563, A58
Wu Y.Z., Zhang W., Zhao Y.H., 2019, MNRAS, 486, 5310
Zenocratti L.J., et al., 2020, MNRAS, 496, L33